Development of the Bethe-Salpeter method considering second-order corrections for a *GW* electron-hole interaction kernel

Satoka Yamada and Yoshifumi Noguchi ●*

Department of Applied Chemistry and Biochemical Engineering, Graduate School of Engineering, Shizuoka University,
3-5-1 Johoku, Hamamatsu, Shizuoka 432-8561, Japan

Kohei Ishii ●, Daichi Hirose, and Osamu Sugino ●

Institute for Solid State Physics, The University of Tokyo, 5-1-5 Kashiwanoha, Kashiwa, Chiba 277-8581, Japan

Kaoru Ohno ●

Department of Physics, Graduate School of Engineering, Yokohama National University, 79-5 Tokiwadai,
Hodogaya, Yokohama 240-8501, Japan

We derive two second-order exchange terms in the *GW* electron-hole interaction kernel. The contributions of these terms have been neglected in the conventional *GW* + Bethe-Salpeter method, and we implement them in an all-electron mixed basis program. To reveal the effect of these terms, we apply them to 28 molecules of Thiel's benchmark set and compare the S_1 excitation energies with those obtained from the conventional *GW* + Bethe-Salpeter method. In addition, using the exciton analysis method with exciton wave functions, we estimate the expectation values for each term in the *GW* electron-hole interaction kernel. The contribution of the two second-order exchange terms is approximately 0.1–0.2 eV at the exciton states of the $n \to \pi^*$ transition; however, the contributions are smaller for the $\pi \to \pi^*$ and $\pi \to$ Rydberg transitions. Our findings reveal that the errors of the conventional *GW* + Bethe-Salpeter method are potentially reduced by considering these terms; however, the extent of the corrections is insufficient for the underestimated excitation energies. We believe that our findings are a significant step towards advancing the conventional *GW* + Bethe-Salpeter method.

I. INTRODUCTION

The Green's function method based on the many-body perturbation theory [1] beyond the density-functional theory (DFT) framework is a powerful first-principles tool that is capable of simulating the accurate excitation energy spectra of a wide range of materials in isolated and extended systems [2–7]. The excitonic states closely related to the photoabsorption spectra and photoemission spectra can be simulated by solving the Bethe-Salpeter equation (BSE) to determine the response function: $L = L_0 + L_0 \Xi^{GW} L$ [8–10]. An electron-hole interaction kernel within the *GW* approximation (GWA) [11] Ξ^{GW} in BSE describes an exciton binding energy and is defined as the functional derivative of Hartree and *GW* one-electron self-energy operators using the one-particle Green's function: $\Xi^{GW} = \frac{\partial}{\partial G}(\Sigma^H + \Sigma^{GW})$. The exciton binding energies can be expressed in this method using four terms: the first term corresponds to the direct dynamically screened Coulombic interaction between excited electrons and holes. The remaining consist of one first- and two second-order exchange terms corresponding to the repulsive Coulombic interactions between electron–hole pairs. The conventional

method has been completely ignores the two second-order exchange terms ($= iG\frac{\partial W}{\partial G}$) based on the assumption that these have negligibly small contributions; however, this has not been confirmed yet [3,8–10], except for Na_2 clusters [12].

Several benchmark tests reveal that errors of the *GW* + BSE method can be estimated for small-sized molecules composed of up to a few tens of atoms compared with other high-level quantum chemistry simulation methods or experimental data [13–26]. The one-shot method has been investigated abundantly as a starting point dependency and revealed that the use of underestimated DFT gaps causes the underestimation of the *GW* gap because of the overscreening problem [6,27,28]. Additionally, we demonstrated that the *GW* + BSE method of one-shot version starting from DFT-LDA underestimates the optical gaps by approximately 1 eV for extremely small sized molecules with significant exciton binding energies (5–12 eV), and we attempted to improve the errors within the framework of the *GW* methods. We concluded that neither the partially self-consistent *GW* nor the complete BSE Hamiltonian without a Tamm-Dancoff approximation could significantly improve the error of 1 eV, and more intrinsic development, particularly for the treatment of the exciton binding energies, is necessary [29]. Recently, Azarias *et al.* [30] focused on the excited states with the

*NOGUCHI.Yoshifumi@shizuoka.ac.jp

045113-1

significant contribution of the $n \to \pi^*$ transition and discussed the functional dependence of errors for several molecules. The authors reported that their one-shot *GW* method underestimated the optical gaps by 0.2–0.3 eV. The more systematic error estimations of the *GW* + BSE method have been performed for the standard organic molecules set (or Thiel's set [31,32]) by several groups [20–26]. According to their benchmark simulations, the *GW* + BSE method underestimates the optical gaps. Therefore, the development of accurate and reliable computational methods is necessary.

Before investigating the beyond-*GW* method [28], we need to arrive at the "exact" *GW* + BSE method that considers the second-order exchange corrections [33]. Estimating and understanding the effect of the second-order exchange corrections is for advancing the conventional *GW* + BSE method. Therefore, we formulate the two second-order exchange terms and implement them in our original all-electron mixed basis program, in which the one-electron wave function is expanded using numerical atomic orbitals and plane waves. Subsequently, we apply these terms to 28 molecules composed of H, C, N, and O [32], and compare the simulated S_1 excitation energies with those obtained from the conventional *GW* + BSE method without the second-order exchange corrections. To reveal the effect of these corrections, we employ the exciton analysis method comprising the exciton wave function and estimate the expected values for the each of the four terms in the *GW* electron-hole interaction kernel. The second-order exchange corrections shows somewhat larger positive values of 0.1–0.2 eV for the S_1 states, in which $n \to \pi^*$ transition is a significant contribution, negative values of approximately -0.1 eV for $\pi \to \pi^*$ transition dominant S_1 states of benzene and naphthalene with flat molecular geometries, and negligible small values ($< +0.05$ eV) for the $\pi \to$ Rydberg transition. In addition, our exciton analysis revealed that the current corrections tend to be proportional to the exciton binding energy: larger corrections for larger exciton binding energy.

This paper is organized as follows: Section II presents a summary of the formulations of the Bethe-Salpeter equation and the two second-order exchange terms, and the exciton analysis methods. Section III presents the comparison between conventional and present *GW* + BSE methods and the results of exciton analysis. We revealed there that the effect of second-order exchange corrections. The main findings are summarized in Sec. IV. Details of the present method's formulation are given in the Appendix.

II. METHODS

This study employs a one-shot *GW* method composed of three-step calculations. The first step is a standard DFT calculation to generate Kohn-Sham orbital energies and Kohn-Sham one-electron wave functions (note that, in general, the one-shot *GW* method depends on the DFT functionals used in the starting point, and the results will also be affected when the self-consistent procedure in *GW* is employed instead of the one-shot version). Additionally, we employ the local density approximation (LDA) in this step. Using the

approximated energies and wave functions, in the second step, we construct the one-particle Green's function (G_0), which is a dynamically screened Coulombic interaction within the random-phase approximation (W_0), and *GW* one-electron self-energy operator ($\Sigma^{GW} = iG_0W_0$). Additionally, we solve Dyson's equation within the GWA ($G = G_0 + G_0\Sigma^{GW}G$) in a one-shot manner. *GW* quasiparticle energies (E^{GW}) are determined with a Z factor as the solutions to the Dyson's equation. In the last step, the BSE for the response function is solved within the GWA; however, an additional approximation is employed in the conventional *GW* + BSE method, as discussed in this section.

A. Bethe-Salpeter equation within the *GW* approximation

Following formulations in this study were all derived within the Tamm-Dancoff approximation. The BSE within the GWA for the response function (L) is

$$L(1, 1'; 2, 2') = L_0(1, 1'; 2, 2')$$

$$+ \int d3d3'd4d4'L_0(1, 1'; 3, 3')\Xi^{GW}(3, 3'; 4, 4')L(4, 4'; 2, 2'),$$
$$\tag{1}$$

where $1 \equiv (x_1, y_1, z_1, t_1)$, L_0 is the lowest-order response function expressed as a simple product of two one-particle Green's functions $[L_0(1, 1'; 2, 2') = -iG(1, 2)G(2', 1')]$. Note that, because we used the one-shot *GW* (or G_0W_0) in this study, the notations of G_0 and G are properly used in this section. The G_0 should be replaced with G when a self-consistent *GW* procedure is employed. The *GW* electron-hole interaction kernel (Ξ^{GW}) is defined as a functional derivative of the Hartree ($\Sigma^H = iG_0v$) and *GW* ($\Sigma^{GW} = iG_0W_0$) one-electron self-energy operators by the one-particle Green's function:

$$\Xi^{GW}(3, 3'; 4, 4') = i\frac{\partial \Sigma^H(3, 3')}{\partial G_0(4, 4')} + i\frac{\partial \Sigma^{GW}(3, 3')}{\partial G_0(4, 4')}$$

$$= K^{ex}(3, 3'; 4, 4') + K^{d}(3, 3'; 4, 4')$$

$$+ K'(3, 3'; 4, 4'), \tag{2}$$

where K^{ex} expressed as

$$K^{ex}(3, 3'; 4, 4') = i\frac{\partial \Sigma^H(3, 3')}{\partial G_0(4, 4')}$$

$$= \delta(3, 3')\delta(4, 4')v(\boldsymbol{r}_3, \boldsymbol{r}_4)\delta(t_3, t_4) \tag{3}$$

is the first-order exchange term for describing the repulsive Coulombic interactions between electron-hole pairs. The remaining two terms on the right-hand side of Eq. (2) are $K^{d} = -W_0 \frac{\partial G_0}{\partial G_0}$ and $K' = -G_0 \frac{\partial W_0}{\partial G_0}$, respectively. The direct term below is a dynamically screened Coulombic interaction between excited electrons and holes. Note that we do not employ the static approximation for the K^{d} term, which takes the limit of $\omega \to 0$ and removes the ω
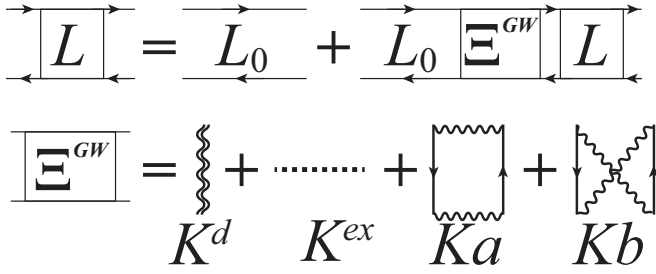
FIG. 1. Feynman diagrams of the BSE and *GW* electron-hole interaction kernel (Ξ^{GW}). The solid line with an arrow denotes the one-particle Green's function, the double wavy line denotes the dynamically screened Coulombic interaction $W(\omega)$, single wavy line denotes the static screened Coulombic interaction [$W(\omega = 0)$], and dotted line denotes the bare Coulomb interaction.

dependence of W_0. The dynamical effect of W_0 was investigated in Refs. [34–37]:

$$K^{d}(3, 3'; 4, 4') = -\delta(3, 4)\delta(3', 4')W_0(3^+, 3'). \quad (4)$$

Using the following relationship:

$$\frac{\partial W_0}{\partial G_0} = \frac{\partial(v + vPW_0)}{\partial G_0} = v\frac{\partial P}{\partial G_0}W_0 + vP\frac{\partial W_0}{\partial G_0} \quad (5)$$

$$= v(1 - vP)^{-1}\frac{\partial P}{\partial G_0}W_0 = W_0\frac{\partial P}{\partial G_0}W_0$$

$$= iW_0\frac{\partial(G_0 G_0)}{\partial G_0}W_0, \quad (6)$$

the K' term can be divided into the two exchange terms ($=Ka^{\text{2nd-ex}} + Kb^{\text{2nd-ex}}$) according to

$$Ka^{\text{2nd-ex}}(3, 3'; 4, 4') = iG(3, 3')G(4, 4^+)$$
$$\times W_0(3^+, 4)W_0(3', 4'), \quad (7)$$

and

$$Kb^{\text{2nd-ex}}(3, 3'; 4, 4') = iG(3, 3')G(4, 4^+)W_0(3^+, 4')W_0(3', 4). \quad (8)$$

These two terms are called the second-order exchange terms in this study. Figure 1 shows the Feynman diagrams of the BSE in Eq. (1) and *GW* electron-hole interaction kernel in Eq. (2).

B. Eigenvalue problem

We solved the BSE via an eigenvalue problem,

$$\sum_{e',o'}\left[(E_e^{GW} - E_o^{GW})\delta_{e,e'}\delta_{o,o'} + K^{d}_{eo,e'o'}\right]A_{e'o'}$$

$$+ 2\sum_{e',o'}\left[K^{\text{ex}}_{eo,e'o'} + Ka^{\text{2nd-ex}}_{eo,e'o'} + Kb^{\text{2nd-ex}}_{eo,e'o'}\right]A_{e'o'} = \Omega_S A_{eo}. \quad (9)$$

The prefactor of two for the exchange terms in Eq. (9) denotes the freedom of spin, i.e., the up-spin electron-hole pair ($e \uparrow$, $o \uparrow$) that can interact with both of ($e' \uparrow$, $o' \uparrow$) and ($e' \downarrow$, $o' \downarrow$) pairs. Furthermore, the freedom of spin is reduced to 1 for the direct (K^{d}) term. The dynamical effect ($\omega \neq 0$) for the K^{d} term is introduced using the generalized plasmon-pole model

[11], and the matrix element of the term is derived in Ref. [3]. Consequently, our K^{d} term and the left-hand-side of Eq. (9) show the Ω_S-dependent form [see also Eq. (B7)]. However, Ω_S as a solution is insensitive to an input Ω_S value. Therefore, we solved Eq. (9) only once as a standard eigenvalue problem by simply setting $\Omega_S = 0$. In this study, we employed a static approximation ($\omega = 0$) for $Ka^{\text{2nd-ex}}$ and $Kb^{\text{2nd-ex}}$ terms but not for K^{d}. These terms can subsequently be expressed as

$$Ka^{\text{2nd-ex}}(3, 3'; 4, 4') \approx iG(3, 3')G(4', 4^+)W_0(3^+, 4)$$
$$\times W_0(3', 4')\delta(t_3^+, t_4)\delta(t_3', t_4'), \quad (10)$$

$$Kb^{\text{2nd-ex}}(3, 3'; 4, 4') \approx iG(3, 3')G(4', 4^+)W_0(3^+, 4')$$
$$\times W_0(3', 4)\delta(t_3^+, t_4')\delta(t_3', t_4), \quad (11)$$

and the corresponding matrix elements are denoted as

$$Ka^{\text{2nd-ex}}_{eo;e'o'} = -\sum_{e_1,o_1}\left[\frac{W_{ee_1;e'o_1}W_{e_1o;o_1o'}}{\Omega_S + (E_o^{GW} - E_{e_1}^{GW}) + (E_{o_1}^{GW} - E_{e'}^{GW})}\right.$$
$$\left. + \frac{W_{eo_1;e'e_1}W_{o_1o;e_1o'}}{\Omega_S - (E_e^{GW} - E_{o_1}^{GW}) - (E_{e_1}^{GW} - E_{o'}^{GW})}\right], \quad (12)$$

$$Kb^{\text{2nd-ex}}_{eo;e'o'} = \left[\sum_{e_1,e_2}\frac{W_{ee_1;e_2o'}W_{e_1o;e'e_2}}{\Omega_S + (E_o^{GW} - E_{e_1}^{GW}) - (E_{e_2}^{GW} - E_{o'}^{GW})}\right.$$
$$\left. + \sum_{o_1,o_2}\frac{W_{eo_1;o_2o'}W_{o_1o;e'o_2}}{\Omega_S - (E_e^{GW} - E_{o_1}^{GW}) + (E_{o_2}^{GW} - E_{e'}^{GW})}\right], \quad (13)$$

where $W_{i,j;k,l}$ is a matrix element of the W_0. The difference between Ka and Kb is the sum of the intermediate states. Ka is the sum of the electrons and holes, and Kb is the sum of the electrons and electrons (holes and holes). The detailed formulas can be found in the Appendix.

C. Exciton analysis

The exciton wave function (Ψ) can be constructed using the eigenvalues A in Eq. (9) and a LDA Kohn-Sham one-electron wave function (ϕ) [38],

$$\Psi_i(r_e, r_h) = \sum_{\nu}^{\text{emp}}\sum_{\mu}^{\text{occ}}A_{\nu,\mu}^i\phi_\nu(\boldsymbol{r}_e)\phi_\mu(\boldsymbol{r}_h), \quad (14)$$

where $\boldsymbol{r}_e$ ($\boldsymbol{r}_h$) and the index (i) denote the coordination of the electrons or holes and the exciton level, respectively. The exciton wave functions include detailed information on the excitons. We can evaluate an expectation value for an arbitrary operator (O) according to:

$$\langle O \rangle_i = \frac{\int d\boldsymbol{r}_e d\boldsymbol{r}_h \Psi_i^*(\boldsymbol{r}_e, \boldsymbol{r}_h)O(\boldsymbol{r}_e, \boldsymbol{r}_h)\Psi_i(\boldsymbol{r}_e, \boldsymbol{r}_h)}{\int d\boldsymbol{r}_e d\boldsymbol{r}_h \Psi_i^*(\boldsymbol{r}_e, \boldsymbol{r}_h)\Psi_i(\boldsymbol{r}_e, \boldsymbol{r}_h)}. \quad (15)$$

The values estimated in this manner indicate the details of the exciton properties in a two-particle picture. We estimate the exciton binding energy (E^{b}) as follows:

$$E^{b} = \langle i|\Xi^{GW}|i\rangle, \quad (16)$$

where Ξ^{GW} is

$$\Xi^{GW} = K^{d} - 2(K^{\text{ex}} + Ka^{\text{2nd-ex}} + Kb^{\text{2nd-ex}}). \quad (17)$$
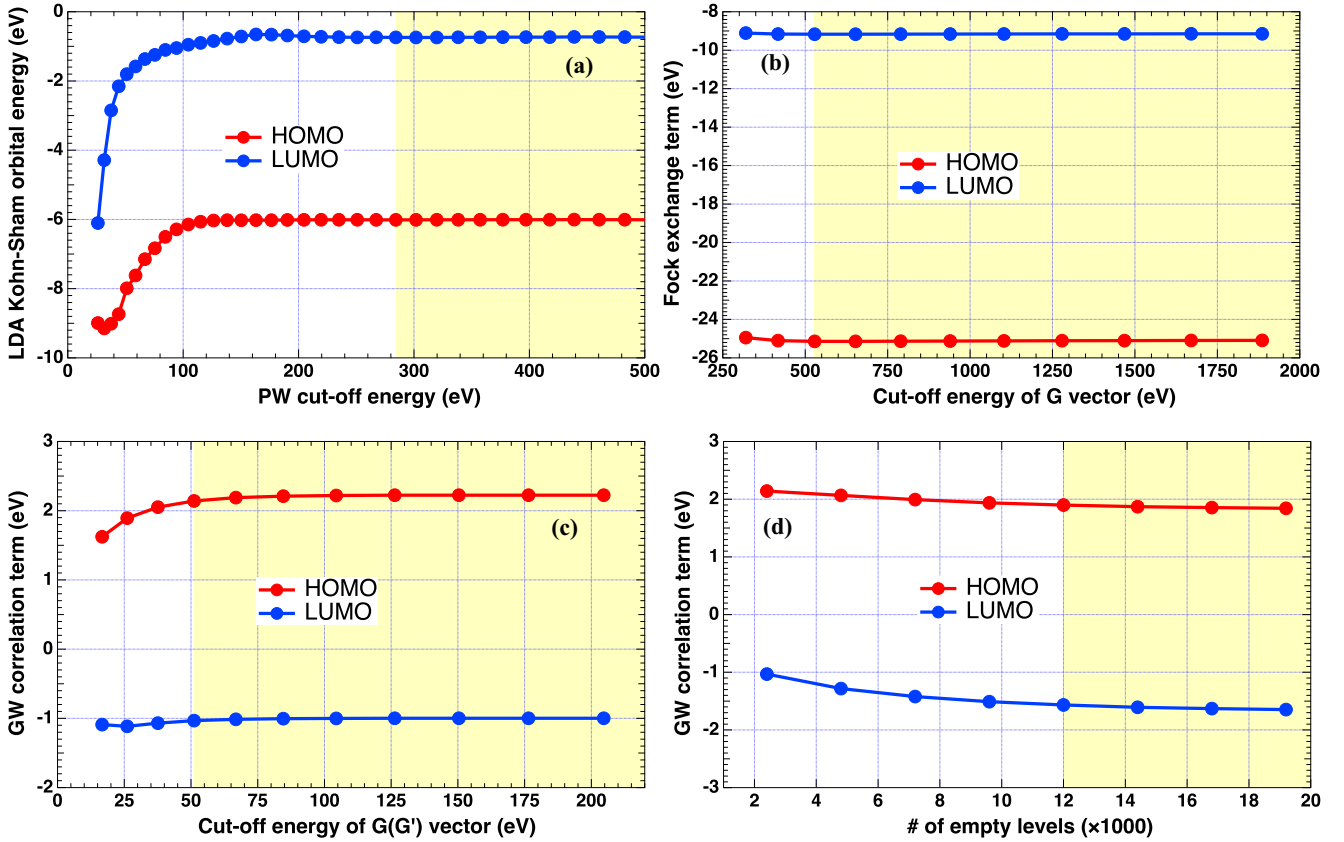
FIG. 2. Convergence behavior of (a) LDA Kohn-Sham orbital energies ($=E^{\text{LDA}}$), (b) Fock-exchange terms ($=iG_0v$), and (c), (d) *GW* correlation terms [$=iG_0(W_0 - v)$] checked for acetamide molecule. See the main text for more details.

Additionally, we estimate the overlap strength of the Kohn-Sham one-electron wave functions at the excited electron and hole states according to

$$\Lambda = \frac{\sum_{e,h} |A_{e,h}^i|^2 \int d\mathbf{r} |\psi_e(\mathbf{r})| |\psi_h(\mathbf{r})|}{\sum_{e,h} |A_{e,h}^i|^2}. \tag{18}$$

In addition, to visualize the exciton states, we estimated the distribution functions of the electrons and holes [39–41] as follows:

$$\Psi_i^e(\mathbf{r}_e) = \int d\mathbf{r}_h |\Psi_i(\mathbf{r}_e, \mathbf{r}_h)|, \tag{19}$$

$$\Psi_i^h(\mathbf{r}_h) = \int d\mathbf{r}_e |\Psi_i(\mathbf{r}_e, \mathbf{r}_h)|. \tag{20}$$

$\Psi_i^e(\mathbf{r}_e)$ [$\Psi_i^h(\mathbf{r}_h)$] is different from that of the Kohn-Sham one-electron wave function because of the excitonic effect from holes (electrons) [39–42].

D. Calculation setup

To systematically discuss the effect of the second-order exchange corrections, we propose a common computational condition comprising 28 molecules in Thiel's set [31,32]. First, we optimize the molecular geometries of the 28 molecules using B3LYP/cc-pVTZ in vacuum [43]. Next, we simulate the S_1 excitation energies of the ground-state molecular geometries using our original all-electron mixed-basis

program [44]. Subsequently, the molecules are placed in similarly sized face-centered-cubic unit cells of a cubic edge of approximately 34 Å. We used large unit cells and a Coulombic cutoff technique [45,46] to completely eliminate the interactions from the molecules in other unit cells. We checked some parameters to get a good convergence for oxygen-included acetamide and employed them for all other molecules because the oxygen-included systems require higher cutoff energies than nitrogen-carbon- or carbon-included systems [6,7,42,47–51]. A PW cutoff energy of 284.3 eV was sufficient to converge the LDA Kohn-Sham orbital energies within 0.01 eV. Additionally, the cutoff energy of **G** vectors is 528.6 eV for the Fock exchange term, and the 51.2 eV cutoff energy of **G** (**G**′) vectors and 12 000 empty states for the *GW* correlation term is sufficient converging the *GW* quasiparticle energies within 0.1 eV. We plotted the behavior of LDA Kohn-Sham orbital energies ($=E^{\text{LDA}}$), Fock-exchange terms ($=iG_0v$), and *GW* correlation terms [$=iG_0(W_0 - v)$] checked for acetamide molecule in Fig. 2. Subsequently, these parameters are used in the Bethe-Salpeter method.

III. RESULTS AND DISCUSSION

Tables I and II show, together with the theoretical best estimates (TBE) [31] for comparison, the S_1 excitation energies simulated using the conventional *GW* + BSE methods, in which the *GW* electron-hole interaction kernel is approximated using the first-order exchange term and the dynamically

TABLE I. Simulated S_1 excitation energies (in eV) and the ratios (in%) at the transition states for the most significant contribution. TBE results [31] are listed for comparison.

	Conventional GW + BSE		Present GW + BSE		TBE
	S_1 (eV)	$n(O) \rightarrow \pi^*$ (%)	S_1 (eV)	$n(O) \rightarrow \pi^*$ (%)	(eV)
Acetamide	4.625	93.0	4.714	93.1	5.80
Acetone	3.261	96.2	3.455	96.5	4.40
Cytosine	4.647	62.4	4.673	61.0	4.87
Formaldehyde	3.106	98.8	3.203	98.8	3.88
Formamide	4.773	99.2	4.862	99.4	5.63
p-Benzoquinone	1.908	90.4	2.038	92.0	2.80
Propanamide	4.211	81.4	4.310	81.3	5.72
Thymine	4.165	79.9	4.251	81.8	4.82
Uracil	4.393	78.9	4.468	81.4	4.80
	S_1 (eV)	$n(N) \rightarrow \pi^*$ (%)	S_1 (eV)	$n(N) \rightarrow \pi^*$ (%)	(eV)
Pyridine	4.202	99.6	4.241	99.6	4.59
Pyrazine	3.572	99.6	3.615	99.6	3.95
Pyridazine	3.347	99.4	3.408	99.4	3.78
Pyrimidine	3.888	99.7	3.925	99.7	4.55
s-Tetrazine	2.120	98.5	2.218	98.9	2.24
s-Triazine	4.181	51.4	4.249	51.8	4.60

screened direct term according to $\Xi^{GW} \sim K^d - 2K^{ex}$. Furthermore, the present GW + BSE is used, in which two second-order exchange terms ($Ka^{2nd\text{-}ex}$ and $Kb^{2nd\text{-}ex}$) are considered in addition to the two terms in the conventional GW + BSE method. The 28 molecules in the Thiel's set are divided into four categories according to the symmetries of the most significant transition states: $n(O) \rightarrow \pi^*$, $n(N) \rightarrow \pi^*$, $\pi \rightarrow \pi^*$, and $\pi \rightarrow$ Rydberg. The n orbital means a noncovalently

bonded electron pair of oxygen or nitrogen atom, thereby localizing around oxygen or nitrogen atom. We denote the n orbitals of oxygen and nitrogen as $n(O)$ and $n(N)$, respectively, in this study. Simultaneously, the π, π^*, and Rydberg orbitals are considered to be delocalized and possess amplitudes covering the entire molecules.

A total of 15 molecules, of which the most significant transition at S_1 is $n \rightarrow \pi^*$, are listed in Table I. The molecules'

TABLE II. Simulated S_1 excitation energies (in eV) and the ratios (in percent) at the transition states for the most significant contribution. TBE results [31] are listed for comparison.

	Conventional GW + BSE		Present GW + BSE		TBE
	S_1 (eV)	$\pi \rightarrow \pi^*$ (%)	S_1 (eV)	$\pi \rightarrow \pi^*$ (%)	(eV)
Benzene	4.795	87.9	4.725	87.9	5.08
Naphthalene	3.898	50.0	3.805	50.0	4.24
Norbomadiene	4.723	56.7	4.737	56.9	5.34
	S_1 (eV)	$\sigma \rightarrow \pi^*$ (%)	S_1 (eV)	$\sigma \rightarrow \pi^*$ (%)	(eV)
Cyclopropene	5.421	96.9	5.488	96.8	6.76
	S_1 (eV)	$\pi \rightarrow$ Rydberg (%)	S_1 (eV)	$\pi \rightarrow$ Rydberg (%)	(eV)
Adenine	4.355	58.6	4.422	61.7	
(All-E)-Hexatriene	4.649	44.3	4.665	44.4	
(All-E)-Octatetraene	4.300	44.2	4.323	44.5	
Cyclopentadiene	4.416	53.9	4.430	54.0	
E-Butadiene	5.165	47.9	5.180	47.9	
Ethene	6.156	51.3	6.169	51.3	
Furan	4.783	47.4	4.795	47.5	
Imidazole	4.716	66.2	4.707	65.9	
Pyrrole	4.069	61.0	4.076	60.8	

93.1 %
$n(O) \longrightarrow \pi^*$

Acetamide

61.0 %
$n(O) \longrightarrow \pi^*$

Cytosine

99.6 %
$n(N) \longrightarrow \pi^*$

Pyradine

51.8 %
$n(N) \longrightarrow \pi^*$
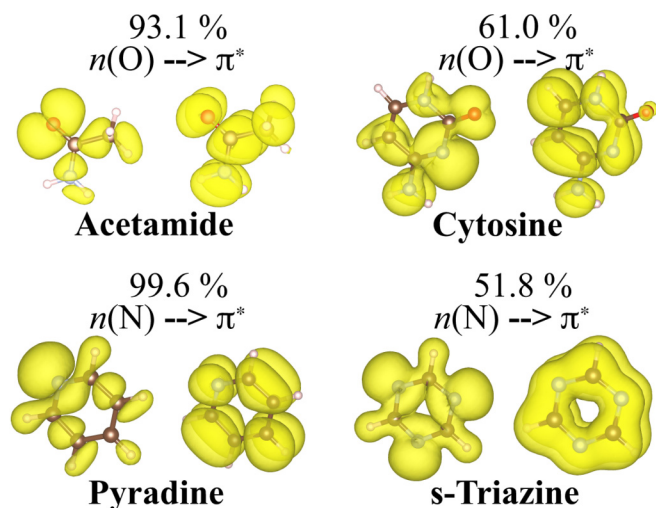

s-Triazine

FIG. 3. Plots of the $\Psi^h(\mathbf{r}_h)$ and $\Psi^e(\mathbf{r}_e)$ for acetamide, cytosine, pyradine, and *s*-Triazine.

S_1 states commonly display weak-state hybridization where the contribution of the $n \to \pi^*$ transition is higher than 80%, except for cytsine (61.0%) and *s*-Triazine (51.8%). Any significant differences between the conventional and present $GW + BSE$ methods cannot be found in either the S_1 excitation energies or ratios of the state hybridizations of these molecules. However, slightly larger energy differences can be observed for $n(O) \to \pi^*$ than for $n(N) \to \pi^*$: the second-order exchange corrections are approximately 0.1–0.2 eV for $n(O) \to \pi^*$ and less than 0.1 eV for $n(N) \to \pi^*$. These energy differences are discussed in detail in a later section. In comparison with TBE [31], the conventional $GW + BSE$ results, as well as those of other previously reported $GW + BSE$ methods [20–26], overestimate the S_1 energies. The second-order exchange corrections improve the S_1 energies; however, this improvement is insufficient; that is, the present $GW + BSE$ results are still underestimated.

As shown in Figs. 3 and 4, π^* characteristics can be commonly observed in the Ψ^e plots for all the molecules (refer to the Supplemental Materials section for further information [52]). The Ψ^h plots clearly reveal the n character of the weak-state hybridized acetamide (93.1%) and pyridine (99.6%); however, this is unclear for cytsine (61%) and *s*-Triazine (51.8%). Notably, Ψ^h and Ψ^e become equal to the Kohn-Sham orbitals ($|\phi(\mathbf{r})|$) at the highest occupied molecular orbital (HOMO) and lowest unoccupied molecular orbital
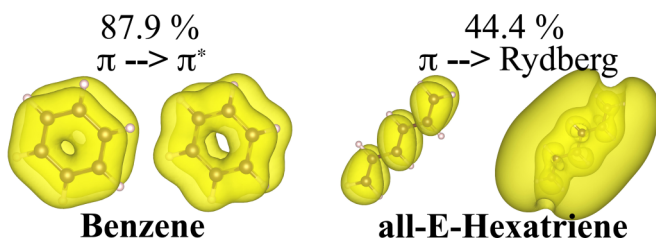
87.9 %
$\pi \longrightarrow \pi^*$

Benzene

44.4 %
$\pi \longrightarrow$ Rydberg

all-E-Hexatriene

FIG. 4. Plots of $\Psi^h(\mathbf{r}_h)$ and $\Psi^e(\mathbf{r}_e)$ for benzene and (all-*E*)-Hexatriene.
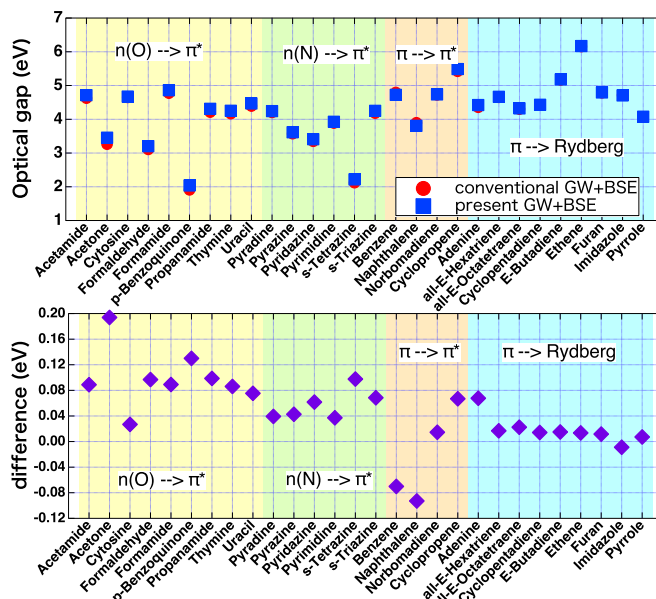

FIG. 5. The optical gap (equal to the S_1 excitation energy) was simulated using the conventional $GW + BSE$ (denoted by the red circle) and present $GW + BSE$ (denoted by the blue square) methods. The lower figure shows the difference between the conventional and present $GW + BSE$; the positive and negative values indicate the positive and negative contributions of the K' term, respectively.

(LUMO) only when the state hybridization does not occur. Ψ^h of acetamide is localized at the oxygen atom as the $2p$ orbital, and the main amplitude is around the oxygen atom. In contrast, the Ψ^h of the strong state hybridized cytosine is delocalized and observing the character of the oxygen $2p$ orbital is difficult.

Table II lists the results of the molecules, of which the most significant transition at S_1 are $\pi \to \pi^*$ and $\pi \to$ Rydberg. Unlike the $n \to \pi^*$ dominant molecules in Table I, strong state hybridizations occur in these molecules, i.e., the ratios of the most significant transition states are less than 66%. The state hybridization is weak only for benzene because the twofold-degenerate π at the HOMO and twofold-degenerate π^* at the LUMO, respectively, i.e., the large contribution of 88.0%, is the result of the strong state hybridization that occurs among these four orbitals. Although significant differences between the conventional and present $GW + BSE$ cannot be found in this case either, the S_1 excitation energies of the present $GW + BSE$ for benzene and naphthalene are approximately 0.1 eV smaller than those obtained for the conventional $GW + BSE$. This is, however, not observed for any other molecule listed in Tables I and II.

We use the $|\Psi^h|$ and $|\Psi^e|$ plots of benzene and (all-*E*)-Hexatriene molecules as typical examples of the S_1 states, of which the most significant transitions are $\pi \to \pi^*$ and $\pi \to$ Rydberg. ($|\Psi^h|$ and $|\Psi^e|$ plots for all other molecules can be found in the Supplemental Materials section [52]). Although the state hybridizations are strong for these molecules, the characteristics of the one-electron Kohn-Sham orbitals, i.e., π and Rydberg, remain clear. This indicates that the
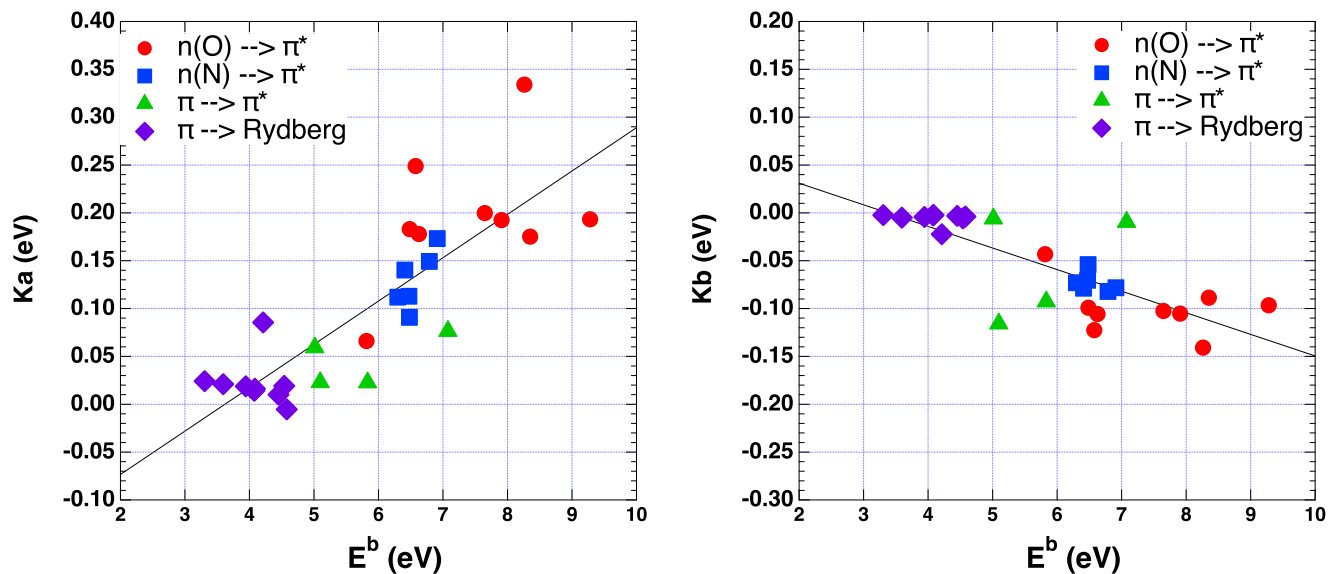
FIG. 6. Expectation values of the exciton binding energy and second-order exchange terms.

state hybridization mainly occurs among other π or Rydberg states [note that, for example, the HOMO and LUMO of benzene are twofold-degenerate π (π^*)]. The contributions of $\pi \to \pi^*$ and $\pi \to$ Rydberg become more significant than other molecules in Table II.

Next, to clarify the effect of the second-order exchange corrections on the S_1 excitation energies, we plot these S_1 excitation energies and the energy differences in Fig. 5. As listed in Tables I and II, the energy differences between the conventional and present GW + BSE are not significant for all the molecules. The tendencies that can be observed in the lower figure are as follows: the largest energy dif-

FIG. 7. Dependence of the first-order exchange (red) and two second-order exchange [Ka (blue) and Kb (green)] terms on Λ values simulated for S_1 states of the 28 molecules. The molecules with a main transition at S_1 state are $n(O) \to \pi^*$ $n(N) \to \pi^*$, $\pi \to \pi^*$, and $\pi \to$ Rydberg, are marked using circles, squares, triangles, and diamonds, respectively.

ferences (0.1–0.2 eV) for $n(O) \to \pi^*$, and large negative contributions for the two completely flat molecular molecules, namely, benzene and naphthalene. The second-order corrections of the absolute values are in order of $n(O) \to \pi^* > n(N) \to \pi^* > \pi \to \pi^* > \pi \to$ Rydberg. However, the corrections are larger for the molecules with flat molecular geometries.

We plotted the expectation values of $Ka^{2\text{nd-ex}}$ and $Kb^{2\text{nd-ex}}$ as a function of the exciton binding energies (E^b) in Fig. 6. Ka and Kb are proportional to E^b. Because of the strongly localized $n(O)$ orbital, for $n(O) \to \pi^*$ dominant S_1, E^b tends to be larger than those of other transitions from the extended $n(N)$ and π orbitals. Ka has a large positive contribution for larger E^b. Although a similar tendency can be observed for $n(N) \to \pi^*$, the contribution of Ka is smaller than that of $n(O)$ because the localization of $n(N)$ is weaker than $n(O)$. Furthermore, because the Rydberg orbitals have the amplitudes outside the molecules, for $\pi \to$ Rydberg, the E^b becomes smaller (<5 eV). In this case, Ka contributes negligibly (<0.05 eV). A similar concept can be applied to Kb, except to the negative sign of Kb. Kb has the largest contribution to $n(O) \to \pi^*$ with the largest E^b and the smallest contribution to $\pi \to$ Rydberg with the smallest E^b. Because Ka and Kb have opposite signs, they canceled each other, making the second-order corrections small [12]. However, because the absolute value of Kb is smaller than Ka, the second-order exchange corrections contribute positively to most molecules in this study (the energy differences are positive in Fig. 5).

As discussed in Fig. 6, the Ka and Kb values are proportional to the exciton binding energies E^b; however, Ka and Kb are not necessarily sensitive to the overlap strength between the excited electron and hole distribution (Λ) [see Eq. (18)]. Figure 7 shows the dependence of the first and second-order exchange terms dependence on the Λ. The Λ values are approximately in order of $\pi \to \pi^* > n(N) \to \pi^* > n(O) \to \pi^* > \pi \to$ Rydberg. As expected, the first-order exchange term is proportional to the Λ because the overlap matrix elements of the excited electron and the hole
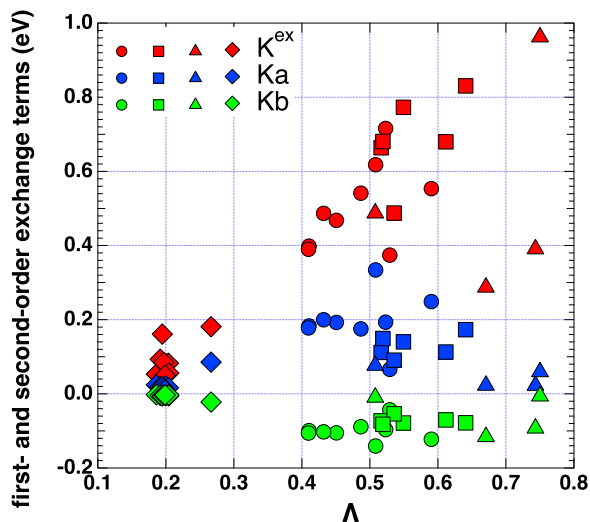
distribution are simulated therein (refer to the Supplemental Material [52]). Ka and Kb are difficult to formulate, and the energy denominators determine the amplitudes of the corrections [Eqs. (7) and (8)]. This behavior can be explained using x-ray absorption spectra (XAS) simulations as a typical example, in which the extremely localized core electron is excited to the empty states. We simulated the XAS for acetone in this study. However, the second-order exchange corrections are not large enough ($\approx$0.7 eV) for O 1s XAS because the overlap matrix in the numerator and the energy denominator on the second-order exchange terms increase. Notably, a correction of approximately 0.7 eV may appear more significant than that of S_1; however, O 1s excitation energy is more than 500 eV. As a final remark of this section, we mention a potential application of the second-order exchange terms for the future work. It is possible that these corrections could improve the description of the double excitation (2h, 2e) energies [26] and hence the satellite peaks more importantly than the single excitation (1h, 1e) as investigated in this study, because the double excitation energies appear in the denominators of Ka and Kb terms [see Eqs. (12) and (13)].

This study simulated the excitation energies of 28 molecules in Thiel's set considering the second-order exchange corrections and revealed the characteristics using the exciton analysis method. The amplitudes of the corrections were sufficiently large to reduce the underestimation errors of 0.2–0.3 eV for $n \to \pi^*$ excitation in the conventional one-shot GW method [30]. However, the amplitudes are not sufficiently large to reduce the detected for the extremely small-sized molecules composed of less than six atoms, which can be up to 1 eV [29]. According to our exciton analysis, the second-order exchange corrections increase for the excitonic states with the large exciton binding energies. We believe that our findings are a significant step towards advancing the conventional GW + BSE method and will be essential knowledge for considering the beyond GW method.

IV. SUMMARY

We derived the two second-order exchange terms (or $iG_0 \frac{\partial W_0}{\partial G_0}$) in the GW electron-hole interaction kernel that has

been estimated for the first time and implemented the terms in our original all-electron mixed basis program. We have applied these terms to 28 molecules in Thiel's set and revealed the effect of the second-order exchange corrections by comparing the conventional and present GW + BSE. The main conclusions are as follows: (1) the corrections resulting from the cancellation of Ka with a positive sign and Kb with a negative sign are insignificant; (2) the corrections increase the S_1 excitation energies for the most of the molecules and decrease the excitation energies for the molecules with completely flat molecular geometries such as benzene and naphthalene; (3) the corrections for $n \to \pi^*$ are large and those for $\pi \to$ Rydberg are negligibly small; (4) Ka and Kb are proportional to the exciton binding energies E^b but not for the overlap strength between the excited electron and hole distribution (Λ) unlike the first-order exchange term K^{ex}. The second-order exchange terms can potentially mitigate the underestimation of optical gaps by the conventional GW + BSE; however, the extent of correction is insufficient. We conclude that the valence excitation have a maximum second-order exchange corrections of ± 0.2 eV. Therefore, the conventional assumption that the second-order exchange corrections have a small effect, and the conventional GW + BSE method based on this assumption should be reasonable; meanwhile, the corrections are not negligible for methods beyond the GW + BSE methods. Although we have considered the second-order exchange corrections in the one-shot GW, an "exact" GW+ Bethe-Salpeter method that satisfies the Baym–Kadanoff conservation law [33] requires a self-consistent procedure. In the future work, we will estimate the second-order exchange terms in the self-consistent GW manner.

APPENDIX A

We start from a definition of electron-hole amplitude,

$$X_S(i, i') = \langle N, 0|T[\psi(i)\psi^\dagger(i')]|N, S\rangle \exp(i\Omega_S t^i/2), \tag{A1}$$

$$\tilde{X}_S(i, i') = \langle N, S|T[\psi(i)\psi^\dagger(i')]|N, 0\rangle \exp(-i\Omega_S t^i/2), \tag{A2}$$

where $t^i = (t_i + t'_i)/2$. If $t_1, t'_1 < t_2, t'_2$ or $t_1, t'_1 > t_2, t'_2$, the-particle Green's function becomes

$$
\begin{aligned}
G_2(1, 1'; 2, 2') = &-\langle N, 0|T[\psi(1)\psi^\dagger(1')]T[\psi(2)\psi^\dagger(2')]|N, 0\rangle \theta(\min(t_1, t'_1) - \max(t_2, t'_2)) \\
&-\langle N, 0|T[\psi(2)\psi^\dagger(2')]T[\psi(1)\psi^\dagger(1')]|N, 0\rangle \theta(\min(t_2, t'_2) - \max(t_1, t'_1)).
\end{aligned}
\tag{A3}
$$

Because $\min(t_1, t'_1) = t^1 - |\tau_1|/2$ and $\max(t_2, t'_2) = t^2 + |\tau_2|/2$, where $\tau_i = t_i - t'_i$, we have $\theta(\min(t_2, t'_2) - \max(t_1, t'_1)) = \theta(t^2 - t^1 - |\tau_1|/2 - |\tau_2|/2)$. Using the completeness relation to Eq. (A3), G_2 becomes

$$G_2(1, 1'; 2, 2') = -\sum_S X_S(\boldsymbol{r}_1, \boldsymbol{r}'_1, \tau_1)\tilde{X}_S(\boldsymbol{r}_2, \boldsymbol{r}'_2, \tau_2) \exp[i\Omega_S(t^2 - t^1)]\theta\left(t^1 - t^2 - \frac{1}{2}|\tau_1| - \frac{1}{2}|\tau_2|\right)$$

$$-\sum_S X_S(\boldsymbol{r}_2, \boldsymbol{r}'_2, \tau_2)\tilde{X}_S(\boldsymbol{r}_1, \boldsymbol{r}'_1, \tau_1)\exp[i\Omega_S(t^1 - t^2)]\theta\left(t^2 - t^1 - \frac{1}{2}|\tau_1| - \frac{1}{2}|\tau_2|\right). \tag{A4}$$

The response function (L) can be defined as a special case of G_2 at limit of $2' \to 2^+$,

$$L(1, 1'; 2, 2^+) = -i\sum_{S\neq 0} X_S(\boldsymbol{r}_1, \boldsymbol{r}'_1, \tau_1)\tilde{X}_S(\boldsymbol{r}_2, \boldsymbol{r}_2, -0^+)\exp[i\Omega_S(t_2 - t^1)]\theta\left(t^1 - t_2 - \frac{1}{2}|\tau_1|\right)$$

$$-i\sum_{S\neq 0} X_S(\boldsymbol{r}_2, \boldsymbol{r}_2, -0^+)\tilde{X}_S(\boldsymbol{r}_1, \boldsymbol{r}'_1, \tau_1)\exp[i\Omega_S(t^1 - t_2)]\theta\left(t_2 - t^1 - \frac{1}{2}|\tau_1|\right), \tag{A5}$$

$$L(1, 1'; \boldsymbol{r}_2, \boldsymbol{r}_2; \omega) \equiv -\int_{-\infty}^{+\infty} dt_2 e^{-i\omega t_2} L(1, 1'; 2, 2^+)$$

$$= -e^{-i\omega(t^1 - |\tau_1|/2)}\sum_{S\neq 0} \frac{X_S(\boldsymbol{r}_1, \boldsymbol{r}'_1, \tau_1)\tilde{X}_S(\boldsymbol{r}_2, \boldsymbol{r}_2, -0^+)}{\omega - \Omega_S + i0^+}e^{-i\Omega_S|\tau_1|/2}$$

$$+ e^{-i\omega(t^1 + |\tau_1|/2)}\sum_{S\neq 0} \frac{X_S(\boldsymbol{r}_2, \boldsymbol{r}_2, -0^+)\tilde{X}_S(\boldsymbol{r}_1, \boldsymbol{r}'_1, \tau_1)}{\omega + \Omega_S - i0^+}e^{-i\Omega_S|\tau_1|/2}. \tag{A6}$$

The first term of right hand side of Eq. (A6) represents the exciton creation process with a positive energy, while the second term represents the exciton recombination process with a negative energy. If $\omega > 0$ and $\omega \sim \Omega_S$, then the corresponding term is only dominant,

$$L(1, 1'; \boldsymbol{r}_2, \boldsymbol{r}_2; \omega) \sim e^{-i\Omega_S t'}\frac{X_S(\boldsymbol{r}_1, \boldsymbol{r}'_1, \tau_1)\tilde{X}_S(\boldsymbol{r}_2, \boldsymbol{r}_2, -0^+)}{\omega - \Omega_S + i0^+}e^{-i\Omega_S|\tau_1|/2}$$

Thus, BSE becomes

$$X_S(\boldsymbol{r}_1, \boldsymbol{r}'_1; \tau_1) = \int d3d3'd4d4' L_0(1, 1'; 3, 3')\Xi(3, 3'; 4, 4')X_S(\boldsymbol{r}_4, \boldsymbol{r}'_4; \tau_4)e^{-i\Omega_S t^4}. \tag{A7}$$

Because of $t_1 \to 0$ for $\tau_1 \to -0^+$, above BSE becomes

$$X_S(\boldsymbol{r}_1, \boldsymbol{r}'_1; -0^+) = \int d3d3'd4d4' L_0(\boldsymbol{r}_1, \boldsymbol{r}'_1; 3, 3')\Xi(3, 3'; 4, 4')X_S(\boldsymbol{r}_4, \boldsymbol{r}'_4; \tau_4)e^{-i\Omega_S t^4}. \tag{A8}$$

Using $\psi(\boldsymbol{r}_1) = \sum_n a_n\phi_n(\boldsymbol{r}_1)$ and defining $A_{e,o} = \langle N, 0|a_e a_o^\dagger|N, S\rangle$ and $B_{e,o} = \langle N, 0|a_o a_e^\dagger|N, S\rangle$, we obtain

$$X_S(\boldsymbol{r}_1, \boldsymbol{r}'_1; \tau_1) = e^{i\Omega_S|\tau_1|/2}\sum_{e,o}\{A_{e,o}\phi_e(\boldsymbol{r}_1)\phi_o^*(\boldsymbol{r}'_1)[\theta(\tau_1)e^{-iE_o\tau_1} + e^{-iE_e\tau_1}\theta(-\tau_1)] + B_{e,o}\phi_o(\boldsymbol{r}_1)\phi_e^*(\boldsymbol{r}'_1)[\theta(\tau_1)e^{-iE_o\tau_1} + e^{-iE_e\tau_1}\theta(-\tau_1)]\}. \tag{A9}$$

The second term on the right-hand side is vanished by Tamm-Dancoff approximation. Equation (A9) can be simplified assuming $\tau_1 = 0^+$,

$$X_S(\boldsymbol{r}_1, \boldsymbol{r}'_1; 0^+) = \sum_{e,o} A_{e,o}\phi_e(\boldsymbol{r}_1)\phi_o^*(\boldsymbol{r}'_1). \tag{A10}$$

Here, we rewrite $L_0(\boldsymbol{r}_1, \boldsymbol{r}'_1; 3, 3') = -iG(\boldsymbol{r}_1, \boldsymbol{r}_3; -t_3)G(\boldsymbol{r}'_3, \boldsymbol{r}'_1; t'_3)$ in explicit form,

$$L_0(\boldsymbol{r}_1, \boldsymbol{r}'_1; 3, 3') = (-i)^3\left[\sum_e \phi_e(\boldsymbol{r}_1)\phi_e^*(\boldsymbol{r}_3)e^{+iE_e t_3}\theta(-t_3) - \sum_o \phi_o(\boldsymbol{r}_1)\phi_o^*(\boldsymbol{r}_3)e^{+iE_o t_3}\theta(t_3)\right]$$

$$\times \left[\sum_e \phi_e(\boldsymbol{r}'_3)\phi_e^*(\boldsymbol{r}'_1)e^{-iE_e t'_3}\theta(t'_3) - \sum_o \phi_o(\boldsymbol{r}'_3)\phi_o^*(\boldsymbol{r}'_1)e^{-iE_o t'_3}\theta(-t'_3)\right]. \tag{A11}$$

Multiplying Eq. (A8) by $\phi_e(\boldsymbol{r}_1)\phi_o(\boldsymbol{r}'_1)$ and integrating with respect to $\boldsymbol{r}_1$ and $\boldsymbol{r}'_1$, we obtain

$$A_{e,o} = -i\int d3d3'd4d4' e^{iE_e t_3}e^{-iE_o t'_3}\theta(-t_3)\theta(-t'_3)\phi_e^*(\boldsymbol{r}_3)\phi_o(\boldsymbol{r}'_3)\Xi(3, 3'; 4, 4')X_S(\boldsymbol{r}_4, \boldsymbol{r}'_4; \tau_4)e^{-i\Omega_S t^4}. \tag{A12}$$

APPENDIX B: CONVENTIONAL $GW + $ BSE METHOD

The conventional $GW + $ BSE method approximates the electron-hole interaction kernel as

$$\Xi^{GW}(3, 3'; 4, 4') \sim \delta(3, 4)\delta(3', 4')v(\boldsymbol{r}_3, \boldsymbol{r}_4)\delta(t_3, t'_4) - \delta(3, 4)\delta(3', 4')W(3^+, 3'). \tag{B1}$$

First, we derive the matrix element of the first-order exchange term. Inserting $K^{ex}(3, 3'; 4, 4') = \delta(3, 3')\delta(4, 4')v(\boldsymbol{r}_3, \boldsymbol{r}_4)\delta(t_3, t_4)$ into Eq. (A12), the matrix elements for the first-order exchange term is

$$
A_{e,o} = -i \int d3 d3' d4 d4' e^{iE_e t_3} e^{-iE_o t_3'} \theta(-t_3)\theta(-t_3') \phi_e^*(\boldsymbol{r}_3)\phi_o(\boldsymbol{r}_3')[\delta(3, 3')\delta(4, 4')v(\boldsymbol{r}_3, \boldsymbol{r}_4)\delta(t_3, t_4)]X_S(\boldsymbol{r}_4, \boldsymbol{r}_4'; \tau_4)e^{-i\Omega_S t^4}
$$

$$
= \frac{1}{\Omega_S - \left(E_e^{GW} - E_o^{GW}\right)} \sum_{e',o'} K_{e,o;e',o'}^{\text{ex}} A_{e',o'}, \tag{B2}
$$

where we used Eq. (A9) and defined

$$
K_{e,o;e',o'}^{\text{ex}} = \int d\boldsymbol{r}_3 d\boldsymbol{r}_4 \phi_e^*(\boldsymbol{r}_3)\phi_o(\boldsymbol{r}_3)v(\boldsymbol{r}_3, \boldsymbol{r}_4)\phi_{e'}(\boldsymbol{r}_4)\phi_{o'}^*(\boldsymbol{r}_4). \tag{B3}
$$

Next, we insert $K^d(3, 3'; 4, 4') = -\delta(3, 4)\delta(3', 4')W(3^+, 3')$ into Eq. (A12) to derive the matrix element for the direct term as well,

$$
A_{e,o} = -i \int d3 d3' d4 d4' e^{iE_e t_3} e^{-iE_o t_3'} \theta(-t_3)\theta(-t_3') \phi_e^*(\boldsymbol{r}_3)\phi_o(\boldsymbol{r}_3')
$$

$$
\times (-\delta(3, 4)\delta(3', 4')W(3^+, 3'))X_S(\boldsymbol{r}_4, \boldsymbol{r}_4'; \tau_4)e^{-i\Omega_S t^4}
$$

$$
= i \int d3 d3' e^{iE_e t_3} e^{-iE_o t_3'} \theta(-t_3)\theta(-t_3') \phi_e^*(\boldsymbol{r}_3)\phi_o(\boldsymbol{r}_3')W(3^+, 3')X_S(\boldsymbol{r}_3, \boldsymbol{r}_3'; \tau_3)e^{-i\Omega_S t^3}
$$

$$
= i \sum_{e',o'} A_{e',o'} \int dt_3 dt_3' e^{iE_e t_3} e^{-iE_o t_3'} \theta(-t_3)\theta(-t_3') W_{e,o;e',o'}(t_3 - t_3')
$$

$$
\times \left(e^{i\Omega_S|\tau_3|/2} [\theta(\tau_3)e^{-iE_{o'}\tau_3} + e^{-iE_{e'}\tau_3}\theta(-\tau_3)] \right) e^{-i\Omega_S t^3}
$$

$$
= i \sum_{e',o'} A_{e',o'} \int dt_3 dt_3' \frac{d\omega}{2\pi} e^{-i\omega 0^+} e^{i\omega(t_3 - t_3')} e^{iE_e t_3} e^{-iE_o t_3'} \theta(-t_3)\theta(-t_3') W_{e,o;e',o'}(\omega)
$$

$$
\times \left(e^{i\Omega_S|\tau_3|/2} [\theta(\tau_3)e^{-iE_{o'}\tau_3} + e^{-iE_{e'}\tau_3}\theta(-\tau_3)] \right) e^{-i\Omega_S t^3}
$$

$$
= i \sum_{e',o'} A_{e',o'} \int \frac{d\omega}{2\pi} e^{-i\omega 0^+} W_{e,o;e',o'}(\omega)
$$

$$
\times \left[\int dt_3 d\tau_3 \theta(-t_3)\theta(\tau_3) e^{-i(\Omega_S - (E_e^{GW} - E_o^{GW}))t_3} e^{i(\Omega_S - \omega - (E_{e'}^{GW} - E_o^{GW}))\tau_3} \right.
$$

$$
\left. + \int dt_3' d\tau_3 \theta(-t_3')\theta(-\tau_3) e^{-i(\Omega_S - (E_e^{GW} - E_o^{GW}))t_3'} e^{-i(\Omega_S + \omega - (E_e^{GW} - E_{o'}^{GW}))\tau_3} \right]
$$

$$
= -\frac{1}{\Omega_S - \left(E_e^{GW} - E_o^{GW}\right)} \sum_{e',o'} K_{e,o;e',o'}^d(\Omega_S) A_{e',o'}, \tag{B4}
$$

$K_{e,o;e',o'}^d(\Omega_S)$ in Eq. (B4) is

$$
K_{e,o;e',o'}^d(\Omega_S) = \frac{i}{2\pi} \sum_l \int d\boldsymbol{r} d\boldsymbol{r}' d\omega e^{i\omega 0^+} \phi_e^*(\boldsymbol{r})\phi_o(\boldsymbol{r}')W(\boldsymbol{r}, \boldsymbol{r}', \omega)\phi_{e'}(\boldsymbol{r})\phi_{o'}^*(\boldsymbol{r}')
$$

$$
\times \left[\frac{1}{\Omega_S - \omega - \left(E_{e'}^{GW} - E_o^{GW}\right) + i0^+} + \frac{1}{\Omega_S + \omega - \left(E_e^{GW} - E_{o'}^{GW}\right) + i0^+} \right], \tag{B5}
$$

where $W(\boldsymbol{r}, \boldsymbol{r}'; \omega)$ can be expanded with plasmon frequency ω_l as

$$
W(\boldsymbol{r}, \boldsymbol{r}', \omega) = \sum_l \frac{\omega_l}{2} W_l(\boldsymbol{r}, \boldsymbol{r}') \left(\frac{1}{\omega - \omega_l + i0^+} - \frac{1}{\omega + \omega_l - i0^+} \right). \tag{B6}
$$

Finally, Eq. (B5) becomes

$$
K_{e,o;e',o'}^d(\Omega_S) = \sum_l \int d\boldsymbol{r} d\boldsymbol{r}' \phi_e^*(\boldsymbol{r})\phi_o(\boldsymbol{r}')W_l(\boldsymbol{r}, \boldsymbol{r}')\phi_{e'}(\boldsymbol{r})\phi_{o'}^*(\boldsymbol{r}')
$$

$$
\times \frac{\omega_l}{2} \left[\frac{1}{\omega_l - \left[\left(E_{e'}^{GW} - E_o^{GW}\right) - \Omega_S\right]} + \frac{1}{\omega_l + \left[\left(E_e^{GW} - E_{o'}^{GW}\right) - \Omega_S\right]} \right]. \tag{B7}
$$

APPENDIX C: PRESENT GW + BSE METHOD

To consider the two second–order exchange corrections, we insert $Ka(3, 3'; 4, 4') = iG(3, 3')G(4', 4^+)W(\mathbf{r}_3, \mathbf{r}_4)W(\mathbf{r}'_3, \mathbf{r}'_4)$
$\delta(t_3^+, t_4)\delta(t'_3, t'_4)$ into Eq. (A12) to obtain the following matrix element:

$$
\begin{aligned}
A_{e,o} = &\int d3d3'd4d4'\, e^{iE_e t_3} e^{-iE_o t'_3}\theta(-t_3)\theta(-t'_3)\phi_e^*(\mathbf{r}_3)\phi_o(\mathbf{r}'_3) \\
&\times [G(3, 3')G(4', 4^+)W(\mathbf{r}_3, \mathbf{r}_4)W(\mathbf{r}'_3, \mathbf{r}'_4)\delta(t_3^+, t_4)\delta(t'_3, t'_4)]X_S(\mathbf{r}_4, \mathbf{r}'_4; \tau_4)e^{-i\Omega_S t^3} \\
= &\sum_{e',o'} A_{e',o'} \int d3d3'd\mathbf{r}_4 d\mathbf{r}'_4\, e^{iE_e t_3} e^{-iE_o t'_3}\theta(-t_3)\theta(-t'_3)\phi_e^*(\mathbf{r}_3)\phi_o(\mathbf{r}'_3) \\
&\times \left[-i\sum_{e_1} e^{-iE_{e_1}^{GW}\tau_3}\phi_{e_1}(\mathbf{r}_3)\phi_{e_1}^*(\mathbf{r}'_3)\theta(\tau_3) + i\sum_{o_1} e^{-iE_{o_1}^{GW}\tau_3}\phi_{o_1}(\mathbf{r}_3)\phi_{o_1}^*(\mathbf{r}'_3)\theta(-\tau_3) \right] \\
&\times \left[-i\sum_{e_2} e^{iE_{e_2}^{GW}\tau_3}\phi_{e_2}(\mathbf{r}'_4)\phi_{e_2}^*(\mathbf{r}_4)\theta(-\tau_3) + i\sum_{o_2} e^{iE_{o_2}^{GW}\tau_3}\phi_{o_2}(\mathbf{r}'_4)\phi_{o_2}^*(\mathbf{r}_4)\theta(\tau_3) \right] \\
&\times W(\mathbf{r}_3, \mathbf{r}_4)W(\mathbf{r}'_3, \mathbf{r}'_4)\phi_{e'}(\mathbf{r}_4)\phi_{o'}^*(\mathbf{r}'_4)\{e^{i\Omega_S|\tau_3|/2}[\theta(\tau_3)e^{-iE_{o'}\tau_3} + e^{-iE_{e'}\tau_3}\theta(-\tau_3)]\}e^{-i\Omega_S t^3}. \quad (C1)
\end{aligned}
$$

Here, we used

$$
G(1, 1') = -i\sum_e e^{-iE_e(t_1-t'_1)}\phi_e(\mathbf{r}_1)\phi_e^*(\mathbf{r}'_1)\theta(t_1 - t'_1) + i\sum_o e^{-iE_o(t_1-t'_1)}\phi_o(\mathbf{r}_1)\phi_o^*(\mathbf{r}'_1)\theta(t'_1 - t_1). \quad (C2)
$$

And since $\theta(\tau)\theta(-\tau) = 0$, Eq. (C1) becomes

$$
\begin{aligned}
A_{e,o} = &\sum_{e',o'} A_{e',o'} \int d3d3'd\mathbf{r}_4 d\mathbf{r}'_4\, e^{iE_e t_3} e^{-iE_o t'_3}\theta(-t_3)\theta(-t'_3)\phi_e^*(\mathbf{r}_3)\phi_o(\mathbf{r}'_3)\left[\sum_{e_1,o_2} e^{-i(E_{e_1}^{GW}-E_{o_2}^{GW})\tau_3}\phi_{e_1}(\mathbf{r}_3)\phi_{e_1}^*(\mathbf{r}'_3)\phi_{o_2}(\mathbf{r}'_4)\phi_{o_2}^*(\mathbf{r}_4)\theta(\tau_3). \right. \\
&\left. + \sum_{o_1,e_2} e^{-i(E_{o_1}^{GW}-E_{e_2}^{GW})\tau_3}\phi_{o_1}(\mathbf{r}_3)\phi_{o_1}^*(\mathbf{r}'_3)\phi_{e_2}(\mathbf{r}'_4)\phi_{e_2}^*(\mathbf{r}_4)\theta(-\tau_3) \right] \\
&\times W(\mathbf{r}_3, \mathbf{r}_4)W(\mathbf{r}'_3, \mathbf{r}'_4)\phi_{e'}(\mathbf{r}_4)\phi_{o'}^*(\mathbf{r}'_4)\{e^{i\Omega_S|\tau_3|/2}[\theta(\tau_3)e^{-iE_{o'}\tau_3} + e^{-iE_{e'}\tau_3}\theta(-\tau_3)]\}e^{-i\Omega_S t^3}. \quad (C3)
\end{aligned}
$$

Here, we define $W_{\alpha,\beta;\gamma,\delta} = \int d\mathbf{r}_1 d\mathbf{r}_2 \phi_\alpha^*(\mathbf{r}_1)\phi_\beta(\mathbf{r}_1)W(\mathbf{r}_1, \mathbf{r}_2)\phi_\gamma(\mathbf{r}_2)\phi_\delta^*(\mathbf{r}_2)$,

$$
\begin{aligned}
A_{e,o} = &\sum_{e',o'} A_{e',o'} \int dt_3 dt'_3\, e^{iE_e t_3} e^{-iE_o t'_3}\theta(-t_3)\theta(-t'_3) \\
&\times \left[\sum_{e_1,o_2} e^{-i(E_{e_1}^{GW}-E_{o_2}^{GW})\tau_3}W_{e,e_1;e',o_2}W_{e_1,o;o_2,o'}e^{-iE_{o'}\tau_3}e^{i\Omega_S\tau_3/2}\theta(\tau_3) \right. \\
&\left. + \sum_{o_1,e_2} e^{-i(E_{o_1}^{GW}-E_{e_2}^{GW})\tau_3}W_{e,o_1;e',e_2}W_{o_1,o;e_2,o'}e^{-iE_{e'}\tau_3}e^{-i\Omega_S\tau_3/2}\theta(-\tau_3) \right]e^{-i\Omega_S t^3} \\
= &\sum_{e',o'} A_{e',o'} \\
&\times \left[\sum_{e_1,o_2} W_{e,e_1;e',o_2}W_{e_1,o;o_2,o'}\int e^{-i(\Omega_S-(E_e^{GW}-E_o^{GW}))t_3}\theta(-t_3)dt_3 \int e^{i(\Omega_S+(E_o^{GW}-E_{e_1}^{GW})+(E_{o_1}^{GW}-E_{e'}^{GW}))\tau_3}\theta(\tau_3) \right. \\
&\left. + \sum_{o_1,e_2} W_{e,o_1;e',e_2}W_{o_1,o;e_2,o'}\int e^{-i(\Omega_S-(E_e^{GW}-E_o^{GW}))t'_3}\theta(-t'_3)dt'_3 \int e^{-i(\Omega_S-(E_e^{GW}-E_{o_1}^{GW})-(E_{e_1}^{GW}-E_{o'}^{GW}))\tau_3}\theta(-\tau_3) \right]d\tau_3 \\
= &\frac{1}{\Omega_S - (E_e^{GW} - E_o^{GW})}\sum_{e',o'} Ka_{e,o;e',o'}^{2nd-ex}A_{e',o'}, \quad (C4)
\end{aligned}
$$

where $Ka^{\text{2nd-ex}}$ is

$$
Ka^{\text{2nd-ex}} = -\sum_{e_1,o_1}\left[\frac{W_{e,e_1;e',o_1}W_{e_1,o;o_1,o'}}{\Omega_S + (E_o^{GW} - E_{e_1}^{GW}) + (E_{o_1}^{GW} - E_{e'}^{GW})} + \frac{W_{e,o_1;e',e_1}W_{o_1,o;e_1,o'}}{\Omega_S - (E_e^{GW} - E_{o_1}^{GW}) - (E_{e_1}^{GW} - E_{o'}^{GW})} \right]. \quad (C5)
$$

Next, we insert $Kb(3, 3'; 4, 4') = iG(3, 3')G(4', 4^+)W(\boldsymbol{r}_3, \boldsymbol{r}_4')W(\boldsymbol{r}_3', \boldsymbol{r}_4)\delta(t_3^+, t_4')\delta(t_3', t_4)$ into Eq. (A12) as well,

$$
A_{e,o} = \int d3\,d3'\,d\boldsymbol{r}_4\,d\boldsymbol{r}_4'\,e^{iE_e t_3}e^{-iE_o t_3'}\theta(-t_3)\theta(-t_3')\phi_e^*(\boldsymbol{r}_3)\phi_o(\boldsymbol{r}_3')G(\boldsymbol{r}_3, \boldsymbol{r}_3'; \tau_3)G(\boldsymbol{r}_4', \boldsymbol{r}_4; \tau_3)W(\boldsymbol{r}_3, \boldsymbol{r}_4')W(\boldsymbol{r}_3', \boldsymbol{r}_4)
$$

$$
\times \sum_{e',o'} A_{e',o'}\phi_{e'}(\boldsymbol{r}_4)\phi_{o'}^*(\boldsymbol{r}_4')X_S(\boldsymbol{r}_4, \boldsymbol{r}_4'; -\tau_3)e^{-i\Omega_S t^3}
$$

$$
= \frac{1}{\Omega_S - (E_e^{GW} - E_o^{GW})}\sum_{e',o'}Kb_{e,o;e',o'}^{\text{2nd-ex}}A_{e',o'}, \tag{C6}
$$

where $Kb^{\text{2nd-ex}}$ is

$$
Kb_{e,o;e',o'}^{2nd-ex} = \sum_{e_1,e_2}\frac{W_{e,e_1;e_2,o'}W_{e_1,o;e',e_2}}{\Omega_S + (E_o^{GW} - E_{e_1}^{GW}) - (E_{e_2}^{GW} - E_{o'}^{GW})} + \sum_{o_1,o_2}\frac{W_{e,o_1;o_2,o'}W_{o_1,o;e',o_2}}{\Omega_S - (E_e^{GW} - E_{o_1}^{GW}) + (E_{o_2}^{GW} - E_{e'}^{GW})}. \tag{C7}
$$

[1] L. Hedin, Phys. Rev. **139**, A796 (1965).

[2] G. Onida, L. Reining, R. W. Godby, R. Del Sole, and W. Andreoni, Phys. Rev. Lett. **75**, 818 (1995).

[3] M. Rohlfing and S. G. Louie, Phys. Rev. B **62**, 4927 (2000).

[4] Y. Noguchi and K. Ohno, Phys. Rev. A **81**, 045201 (2010).

[5] Y. Noguchi, O. Sugino, M. Nagaoka, S. Ishii, and K. Ohno, J. Chem. Phys. **137**, 024306 (2012).

[6] Y. Noguchi, O. Sugino, H. Okada, and M. Matsuo, J. Phys. Chem. C **117**, 15362 (2013).

[7] Y. Noguchi, M. Hiyama, H. Akiyama, and N. Koga, J. Chem. Phys. **141**, 044309 (2014).

[8] G. Strinati, Phys. Rev. Lett. **49**, 1519 (1982).

[9] G. Strinati, Phys. Rev. B **29**, 5718 (1984).

[10] G. Strinati, Riv. Nuovo Cimento **11**, 1 (1986).

[11] M. S. Hybertsen and S. G. Louie, Phys. Rev. B **34**, 5390 (1986).

[12] K. Ohno, Sci. Tech. Adv. Mater. **5**, 603 (2004).

[13] J. M. Garcia-Lastra and K. S. Thygesen, Phys. Rev. Lett. **106**, 187402 (2011).

[14] X. Blase and C. Attaccalite, Appl. Phys. Lett. **99**, 171909 (2011).

[15] D. Rocca, D. Lu, and G. Galli, J. Chem. Phys. **133**, 164109 (2010).

[16] D. Rocca, M. Voros, A. Gali, and G. Galli, J. Chem. Theory Comput. **10**, 3290 (2014).

[17] Y. Ma, M. Rohlfing, and C. Molteni, Phys. Rev. B **80**, 241405(R) (2009).

[18] C. Rostgaard, K. W. Jacobsen, and K. S. Thygesen, Phys. Rev. B **81**, 085103 (2010).

[19] C. Faber, C. Attaccalite, V. Olevano, E. Runge, and X. Blase, Phys. Rev. B **83**, 115123 (2011).

[20] D. Jacquemin, I. Duchemin, and X. Blase, J. Chem. Theory Comput. **11**, 3290 (2015).

[21] F. Bruneval, S. M. Hamed, and J. B. Neaton, J. Chem. Phys. **142**, 244101 (2015).

[22] N. L. Nguyen, H. Ma, M. Govoni, F. Gygi, and G. Galli, Phys. Rev. Lett. **122**, 237402/ (2019).

[23] C. Liu, J. Kloppenburg, Y. Yao, X. Ren, H. Appel, Y. Kanai, and V. Blum, J. Chem. Phys. **152**, 044105 (2020).

[24] C. Holzer and W. Klopper, J. Chem. Phys. **149**, 101101 (2018).

[25] J. D. Elliott, N. Colonna, M. Marsili, N. Marzari, and P. Umari, J. Chem. Theory Comput. **15**, 3710 (2019).

[26] S. J. Bintrim and T. C. Berkelbach, J. Chem. Phys. **156**, 044114 (2022).

[27] X. Blase, C. Attaccalite, and V. Olevano, Phys. Rev. B **83**, 115103 (2011).

[28] R. Kuwahara, Y. Noguchi, and K. Ohno, Phys. Rev. B **94**, 121116(R) (2016).

[29] D. Hirose, Y. Noguchi, and O. Sugino, Phys. Rev. B **91**, 205111 (2015).

[30] C. Azarias, C. Habert, Š. Budzaá, X. Blase, I. Duchemin, and D. Jacquemin, J. Phys. Chem. A **121**, 6122 (2017).

[31] M. R. Silva-Junior and W. Thiel, J. Chem. Theory Comput. **6**, 1546 (2010).

[32] M. Schreiber, M. R. Silva-Junior, S. P. A. Sauer, and W. Thiel, J. Chem. Phys. **128**, 134110 (2008).

[33] G. Baym and L. P. Kadanoff, Phys. Rev. **124**, 287 (1961).

[34] A. Marini and R. Del Sole, Phys. Rev. Lett **91**, 176402 (2003).

[35] S. Albrecht, L. Reining, R. Del Sole, and G. Onida, Phys. Rev. Lett. **80**, 4510 (1998).

[36] L. X. Benedict, E. L. Shirley, and R. B. Bohn, Phys. Rev. Lett. **80**, 4514 (1998).

[37] G. Onida, L. Reining, and A. Rubio, Rev. Mod. Phys. **74**, 601 (2002).

[38] D. Hirose, Y. Noguchi, and O. Sugino, J. Chem. Phys. **146**, 044303 (2017).

[39] M. Head-Gordon, A. M. Grafia, D. Maurice, and C. A. White, J. Phys. Chem. **99**, 14261 (1995).

[40] F. Plasser, M. Wormit, and A. Dreuw, J. Chem. Phys. **141**, 024106 (2014).

[41] F. Plasser, M. Wormit, and A. Dreuw, J. Chem. Phys. **141**, 024107 (2014).

[42] Y. Noguchi, J. Chem. Phys. **155**, 204302 (2021).

[43] M. J. Frisch, G. W. Trucks, H. B. Schlegel, G. E. Scuseria, M. A. Robb, J. R. Cheeseman, G. Scalmani, V. Barone, B. Mennucci, G. A. Petersson *et al.*, *Gaussian 09 Revision C.1* (Gaussian, Inc., Wallingford, 2004).

[44] S. Ono, Y. Noguchi, R. Sahara, Y. Kawazoe, and K. Ohno, Comput. Phys. Commun. **189**, 20 (2015).

[45] A. Castro, A. Rubio, and M. J. Stott, Can. J. Phys. **81**, 1151 (2003).

[46] C. A. Rozzi, D. Varsano, A. Marini, E. K. U. Gross, and A. Rubio, Phys. Rev. B **73**, 205119 (2006).

[47] Y. Noguchi and O. Sugino, J. Chem. Phys. **142**, 064313 (2015).

[48] Y. Noguchi, M. Hiyama, H. Akiyama, Y. Harada, and N. Koga, J. Chem. Theory Comput. **11**, 1668 (2015).

[49] Y. Noguchi and O. Sugino, J. Chem. Phys. **146**, 144304 (2017).

[50] Y. Noguchi and O. Sugino, J. Phys. Chem. C **121**, 20687 (2017).

[51] Y. Noguchi, D. Hirose, and O. Sugino, Eur. Phys. J. B **91**, 125 (2018).

[52] See Supplemental Material at http://link.aps.org/supplemental/10.1103/PhysRevB.106.045113 for the detailed formulations of $GW+$ Bethe-Salpeter method, the plots of Ψ^e and Ψ^h for all the molecules, and the expectation values of first- and second-exchange terms.